Second order H-PML for anisotropic forward wavefield simulation

Junxiao Li, Kris Innanen and Bing Wang

ABSTRACT

The Hybrid perfectly matched layer (H-PML) is extended to simulate second order displacement-stress elastic wave equations. In this report, the simulation results with both H-PML and C-PML in isotropic and anisotropic media are compared. H-PML is capable of absorbing boundary reflections in both isotropic and anisotropic media, but the C-PML only works perfectly in isotropic media. The simulation results with H-PML for both first order and second order elastic wave equations show its efficiency in boundary reflections suppression.

INTRODUCTION

For numerical simulations of elastic wave equations, absorbing boundary conditions (ABCs) are needed at the truncated boundaries to suppress the artificial reflections. The PML approach to boundary absorption, introduced by Berenger (1994), has been proven to be very efficient compared with previously developed methods (Collino and Tsogka, 2001; Komatitsch and Tromp, 2003; Festa and Vilotte, 2005). The original PML has two main imperfections: 1) the velocity and stress fields are required to be split into two subfields respectively; and 2) its efficiency decreases at grazing incidence after discretization, because the damping coefficient is inversely proportional to the angular frequency and thus depends on the direction of propagation of the wave. In order to improve the response of the discrete PML at grazing incidence, the convolutional PML (or C-PML) method (Kuzuoglu and Mittra, 1996) or the complex frequency shifted-PML (CFS-PML) method (Bérenger, 2002) can be invoked. The CFS-PML method introduces a frequency-dependent term which eliminates the requirement that the velocity-stress equation be split into separate terms. However, this C-PML is not stable in anisotropic media. The multiaxial perfectly matched layer (M-PML) method has been found to be stable even for media exhibiting very large degrees of anisotropy (Meza-Fajardo and Papageorgiou, 2008). But its absorbing capability in isotropic is less effective compared with the C-PML. To maximize both accuracy and stability, a hybrid PML (H-PML) method, that combines the advantages of both the C-PML and the M-PML through the optimization of the damping profile is proposed (Li et al., 2017).

As the classical PML and PML methods discussed above were primarily designed for first-order equation system, they cannot be applied to the second-order system directly. However, the first-order wave equations are based on the iterations of velocity and stress components. This implies when the first-order based wave equations are used into full waveform inversion (FWI), the velocity components should be transformed into displacement components to calculate the misfit function. It is necessary to develop a PML for the second order wave equations. Komatitsch and Tromp (2003) first proposed the split PML to the second-order seismic wave equation. In 2009, Pinton et al. (2009) proposed an unsplit PML for the second-order acoustic equation and it was used in ultrasonic imag-

ing simulation. But third-order temporal partial derivatives have to be calculated. Liu et al. (2012) further improved this method. However, it's difficult be applied in the implementation of C-PML. Li and Bou Matar (2010) proposed a C-PML for the second-order elastic wave equations, yet he mentioned the instabilities of this method to be applied into anisotropic medium. Ping et al. (2014) presented an M-PML for the second-order elastic wave equation, but the wave fields are required to be split. In this paper, the H-PML are implemented to the second-order wave equations in both isotropic and anisotropic media. Its comparisons with the C-PML for second-order elastic wave equations and the H-PML for first-order elastic wave equations proves its stability in reducing boundary reflections.

SECOND ORDER ELASTIC WAVE EQUATION

Wave propagation in an elastic medium is governed by the equation:

$$\rho \partial_t^2 u_j = \sigma_{ij,j}, \tag{1}$$

where $i, j = 1, 2, 3$, ρ is the density, u_i is the displacement vector and σ_{ij} is stress tensor, and where $\sigma_{ij,j}$ represent spatial derivatives of the stress tensor. The comma between subscripts is used for spatial derivatives. The summation convention for repeated subscripts is assumed. According to Hooke's law, the relationship between the stress and strain tensors is,

$$\sigma_{ij} = c_{ijkl} \varepsilon_{kl}, \tag{2}$$

where c_{ijkl} are the elastic stiffness coefficients. The strain tensor ε_{kl} is

$$\varepsilon_{kl} = \frac{1}{2}(u_{k,l} + u_{l,k})., \tag{3}$$

In the case of a transverse isotopic medium, the second-order wave equation system can be written as,

$$
\begin{aligned}
\frac{\partial^2 u_1}{\partial t^2} &= \frac{1}{\rho}\left(\frac{\partial \sigma_{11}}{\partial x} + \frac{\partial \sigma_{12}}{\partial y} + \frac{\partial \sigma_{13}}{\partial z}\right) \\[2mm]
\frac{\partial^2 u_2}{\partial t^2} &= \frac{1}{\rho}\left(\frac{\partial \sigma_{21}}{\partial x} + \frac{\partial \sigma_{22}}{\partial y} + \frac{\partial \sigma_{23}}{\partial z}\right) , \\[2mm]
\frac{\partial^2 u_3}{\partial t^2} &= \frac{1}{\rho}\left(\frac{\partial \sigma_{31}}{\partial x} + \frac{\partial \sigma_{32}}{\partial y} + \frac{\partial \sigma_{33}}{\partial z}\right)
\end{aligned}
\tag{4}
$$

and

$$\sigma_{11} = c_{11}\frac{\partial u_1}{\partial x} + (c_{11} - 2c_{66})\frac{\partial u_2}{\partial y} + c_{13}\frac{\partial u_3}{\partial z}$$

$$\sigma_{22} = (c_{11} - 2c_{66})\frac{\partial u_1}{\partial x} + c_{11}\frac{\partial u_2}{\partial y} + c_{13}\frac{\partial u_3}{\partial z}$$

$$\sigma_{33} = c_{13}\frac{\partial u_1}{\partial x} + c_{13}\frac{\partial u_2}{\partial y} + c_{33}\frac{\partial u_3}{\partial z}$$

$$\sigma_{23} = c_{44}\left(\frac{\partial u_2}{\partial z} + \frac{\partial u_3}{\partial y}\right) \tag{5}$$

$$\sigma_{13} = c_{44}\left(\frac{\partial u_1}{\partial z} + \frac{\partial u_3}{\partial x}\right)$$

$$\sigma_{12} = c_{66}\left(\frac{\partial u_1}{\partial y} + \frac{\partial u_2}{\partial x}\right),$$

H-PML FOR SECOND ORDER ELASTIC WAVE EQUATIONS

In H-PML, for the new operator $\nabla_{\tilde{x}} = [\frac{\partial}{\partial \tilde{x}}, \frac{\partial}{\partial y}, \frac{\partial}{\partial z}]$, where, $\frac{\partial}{\partial \tilde{x}} = \frac{1}{s_x}\frac{\partial}{\partial x}$, $\frac{\partial}{\partial \tilde{y}} = \frac{1}{s_y}\frac{\partial}{\partial y}$ and $\frac{\partial}{\partial \tilde{z}} = \frac{1}{s_z}\frac{\partial}{\partial z}$. The complex frequency shifted stretched-coordinate matrices s_x, s_y and s_z are

$$s_x = \kappa_x + \frac{d_x + m_{x/y}d_y + m_{x/z}d_z}{\alpha_x + i\omega}$$

$$s_y = \kappa_y + \frac{m_{y/x}d_x + d_y + m_{y/z}d_z}{\alpha_y + i\omega} \tag{6}$$

$$s_z = \kappa_z + \frac{m_{z/x}d_x + m_{z/y}d_y + d_z}{\alpha_z + i\omega},$$

where, $\kappa_x, \kappa_y, \kappa_z$ are real and ≥ 1, d_x, d_y, d_z are damping profiles, ω is angular frequency and $\alpha_x, \alpha_y, \alpha_z$ are assumed to be positive and real. The additional damping profiles $m_{i/j}$ ($i, j = 1, 2, 3, i \neq j$) are weighting factors. When $\kappa_x = 1$ and $\alpha_x = 0$, the C-PML degenerates to the classic PML case (Berenger, 1994). When $m_{i/j} = 0$, we get the C-PML (Kuzuoglu and Mittra, 1996). Using the complex coordinate variables $\tilde{x}, \tilde{y}, \tilde{z}$ to replace the original coordinate variables in (4) and (5), we obtain new displacement-stress equation system in frequency domain

$$-\omega^2 \hat{u}_1 = \frac{1}{\rho}\left(\frac{1}{s_x}\frac{\partial \hat{\sigma}_{11}}{\partial x} + \frac{1}{s_y}\frac{\partial \hat{\sigma}_{12}}{\partial y} + \frac{1}{s_z}\frac{\partial \hat{\sigma}_{13}}{\partial z}\right)$$

$$-\omega^2 \hat{u}_2 = \frac{1}{\rho}\left(\frac{1}{s_x}\frac{\partial \hat{\sigma}_{21}}{\partial x} + \frac{1}{s_y}\frac{\partial \hat{\sigma}_{22}}{\partial y} + \frac{1}{s_z}\frac{\partial \hat{\sigma}_{23}}{\partial z}\right) , \tag{7}$$

$$-\omega^2 \hat{u}_3 = \frac{1}{\rho}\left(\frac{1}{s_x}\frac{\partial \hat{\sigma}_{31}}{\partial x} + \frac{1}{s_y}\frac{\partial \hat{\sigma}_{32}}{\partial y} + \frac{1}{s_z}\frac{\partial \hat{\sigma}_{33}}{\partial z}\right)$$

and

$$\hat{\sigma}_{11} = \frac{1}{s_x}c_{11}\frac{\partial \hat{u}_1}{\partial x} + \frac{1}{s_y}(c_{11} - 2c_{66})\frac{\partial \hat{u}_2}{\partial y} + \frac{1}{s_z}c_{13}\frac{\partial \hat{u}_3}{\partial z}$$

$$\hat{\sigma}_{22} = \frac{1}{s_x}(c_{11} - 2c_{66})\frac{\partial \hat{u}_1}{\partial x} + \frac{1}{s_y}c_{11}\frac{\partial \hat{u}_2}{\partial y} + \frac{1}{s_z}c_{13}\frac{\partial \hat{u}_3}{\partial z}$$

$$\hat{\sigma}_{33} = \frac{1}{s_x}c_{13}\frac{\partial \hat{u}_1}{\partial x} + \frac{1}{s_y}c_{13}\frac{\partial \hat{u}_2}{\partial y} + \frac{1}{s_z}c_{33}\frac{\partial \hat{u}_3}{\partial z} \tag{8}$$

$$\hat{\sigma}_{23} = c_{44}\left(\frac{1}{s_z}\frac{\partial \hat{u}_2}{\partial z} + \frac{1}{s_y}\frac{\partial \hat{u}_3}{\partial y}\right)$$

$$\hat{\sigma}_{13} = c_{44}\left(\frac{1}{s_z}\frac{\partial \hat{u}_1}{\partial z} + \frac{1}{s_x}\frac{\partial \hat{u}_3}{\partial x}\right)$$

$$\hat{\sigma}_{12} = c_{66}\left(\frac{1}{s_y}\frac{\partial \hat{u}_1}{\partial y} + \frac{1}{s_x}\frac{\partial \hat{u}_2}{\partial x}\right),$$

where $\hat{u}, \hat{\sigma}$ represent the Fourier transform of u and σ.

In order to get the H-PML formulation in time domain, equation set (7) and (8) should be transformed back to time domain by inverse Fourier transform. Take the first equation of equation set (7) as an example, we rewrite it by adding convolutional terms as

$$\frac{\partial^2 u_1}{\partial t^2} = \frac{1}{\rho}\left(DFT^{-1}\left[\frac{1}{s_x}\right] * \frac{\partial \sigma_{11}}{\partial x} + DFT^{-1}\left[\frac{1}{s_y}\right] * \frac{\partial \sigma_{12}}{\partial y} + DFT^{-1}\left[\frac{1}{s_z}\right] * \frac{\partial \sigma_{13}}{\partial z}\right), \tag{9}$$

where $*$ denotes convolution and DFT^{-1} is inverse Fourier transform. This equation means the new differential operator in the x direction emerges as

$$\partial_{\tilde{x}} = DFT^{-1}\left[\frac{1}{s_x}\right] * \partial_x. \tag{10}$$

According to Roden and Gedney (2000); Komatitsch and Martin (2007), the inverse Fourier transform term $DFT^{-1}\left[\frac{1}{s_x}\right]$ is

$$DFT^{-1}\left[\frac{1}{s_x}\right] = \frac{\delta t}{\kappa_x} - \frac{d_x}{\kappa_x^2}e^{-(d_x/\kappa_x + \alpha_x)t}H(t) = \frac{\delta t}{\kappa_x} + \zeta_x(t), \tag{11}$$

where δt and $H(t)$ are Dirac delta and Heaviside distributions, respectively. The operator in equation (10) now becomes

$$\partial_{\tilde{x}} = \frac{1}{\kappa_x}\partial_x + \zeta_x(t) * \partial_x. \tag{12}$$

Komatitsch and Martin (2007) replace equation (12) with

$$\partial_{\tilde{x}} = \frac{1}{\kappa_x}\partial_x + \psi_x, \tag{13}$$

where ψ_x is a memory variable updated at each time step n:

$$\psi_x^n = b_x\psi_x^{n-1} + c_x(\partial_x)^{n-1/2}, \tag{14}$$

in which

$$
b_x = \exp\left[- \left(\frac{d_x + m_{x/y}d_y + m_{x/z}d_z}{\kappa_x + \alpha_x} \right) \triangle t \right]
$$
$$
c_x = \left[\frac{d_x + m_{x/y}d_y + m_{x/z}d_z}{\kappa_x \left(d_x + m_{x/y}d_y + m_{x/z}d_z \right) + \kappa_x \alpha_x} \right] (b_x - 1).
$$

(15)

Therefore, equation (9) in time domain can further be expressed as

$$
\frac{\partial^2 u_1}{\partial t^2} = \frac{1}{\rho} \left(\frac{1}{\kappa_x} \frac{\partial \sigma_{11}}{\partial x} + \psi_x \sigma_{11} + \frac{1}{\kappa_y} \frac{\partial \sigma_{12}}{\partial y} + \psi_y \sigma_{12} + \frac{1}{\kappa_z} \frac{\partial \sigma_{13}}{\partial x} + \psi_z \sigma_{13} \right).
$$

(16)

And the first equation of equation set (8) can be rewriten as

$$
\sigma_{11} = c_{11} \left(\frac{1}{\kappa_x} \frac{\partial u_1}{\partial x} + \psi_x u_1 \right) + (c_{11} - 2c_{66}) \left(\frac{1}{\kappa_y} \frac{\partial u_2}{\partial y} + \psi_y u_2 \right)
$$
$$
+ c_{13} \left(\frac{1}{\kappa_z} \frac{\partial u_3}{\partial z} + \psi_y u_3 \right).
$$

(17)

NUMERICAL TEST

In this section, we will first compare C-PML and H-PML applied in the second order elastic wave equation. Then, comparisons between the first order velocity-stress elastic wave field simulation and second order displacement-stress elastic wave simulation in VTI media with H-PML will be discussed.

C-PML and H-PML in isotropic layered medium

In order to demonstrate the difference between C-PML and H-PML in second order elastic wave equations, numerical simulations of elastic wave propagation in layered isotropic medium are presented. The calculation domain (including $25 \times 5m$ PMLs) is 1750 m width and 1750 m height. The properties of the elastic media are in Table 1.

Table 1. Parameters of layered model

	$V_P(m/s)$	$V_S(m/s)$	$\rho(g/cm^3)$
First layer	2500	1300	1.6
Second layer	3257	1377	2.25
Third layer	2000	1200	1.5

A directional point source located at (135 m, 935 m), is loaded on displacement component towards X direction. The point source is the derivative of a Ricker wavelet given by
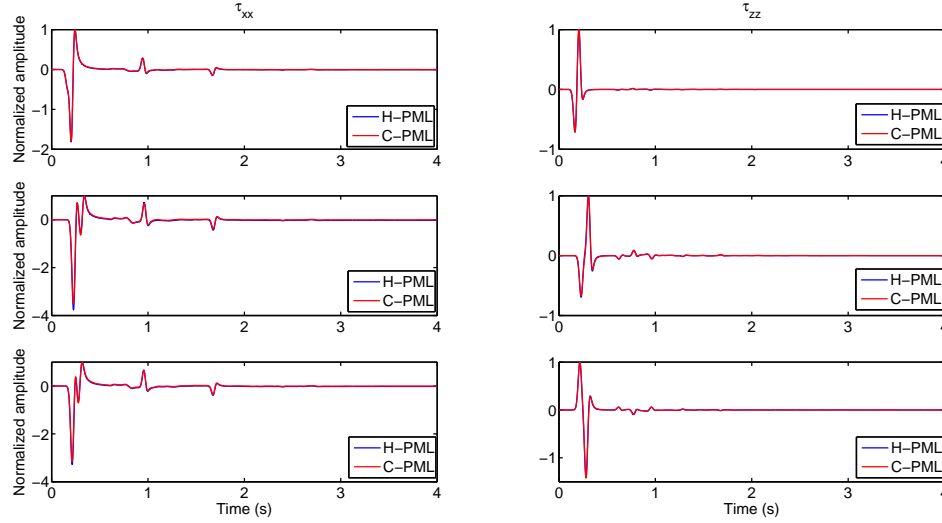
FIG. 1. Waveform comparison of second-order elastic wave equations when H-PML and C-PML are applied respectively. In isotropic media, both the PMLs can provide satisfactory results.

$$f\left(t\right) = A_0(2\pi^2 F_0^2)e^{(-\pi^2 F_0^2(t-t_0)^2)} + 8A_0 t(\pi^4 F_0^4)(t-t_0)^3 e^{(-\pi^2 F_0^2(t-t_0)^2)}, \qquad (18)$$

in which, t_0 is the source delay, F_0 is the central frequency A_0 is the source amplitude.

The corresponding Ricker wavelet is

$$f\left(t\right) = A_0(2\pi^2 F_0^2)(t-t_0)e^{(-\pi^2 F_0^2(t-t_0)^2)}. \qquad (19)$$

In this paper, for the second order displacement-stress wave equations, we apply the point source in equation (18) to the displacement components. And for the first order velocity-stress wave equations, because the relationship between displacement and normal stress components ($\frac{\partial u_i}{\partial x_i} = v_i$, $i = x, y, z$.), we put the point source of the Ricker wavelet in equation (19) on the velocity components instead.

The time evolutions of the normal stress components τ_{xx} (Left) and τ_{zz} (Right) for three receivers are plotted in Figure (1). Simulations with C-PML (red line) matches perfectly with simulations with H-PML (blue line). This is in accordance with Li's results (Li et al., 2017) (both C-PML and H-PML are capable of absorbing boundary reflections effectively in isotropic medium). In second order displacement-stress wave equations, they have almost the same absorbing efficiency. In Figure (2), the snapshots of wave propagation in the layered model with H-PML are also plotted.

Comparisons between C-PML and H-PML in anisotropic media

The second example is for a VTI model. The formation elastic parameters and the density are $c_{11} = 23.87e9N/m^2$, $c_{13} = 9.79e9N/m^2$, $c_{33} = 15.33e9N/m^2$, $c_{44} = 2.77e9N/m^2$ and $\rho = 2000kg/m^3$. The time step is $1ms$, and a directional point source located in the middle of this model is added on displacement component towards X direction.
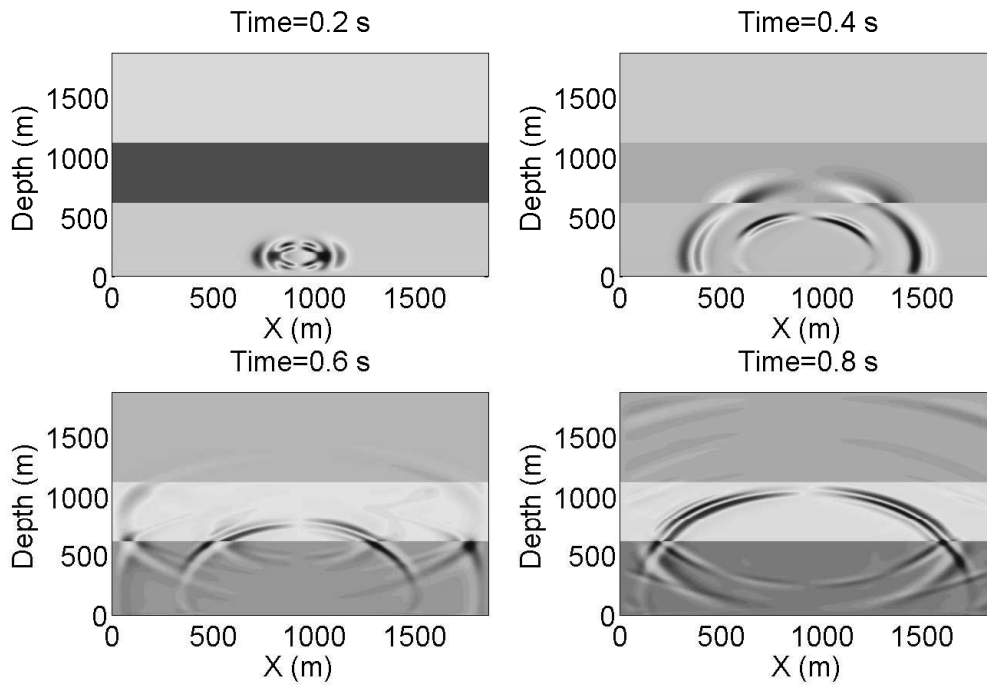
FIG. 2. Snapshots of the stress σ_{xx} in isotropic layered model when H-PML is applied.
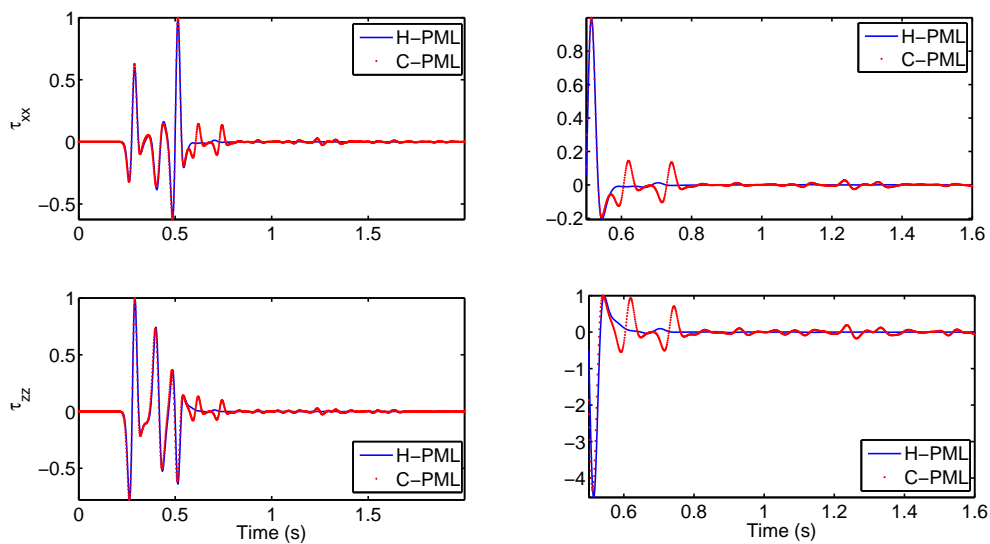

FIG. 3. Waveform comparison of second-order elastic wave equations when H-PML and C-PML are applied respectively in anisotropic media. In anisotropic media, obvious boundary reflections can be detected when C-PML is used as absorbing boundary layers .
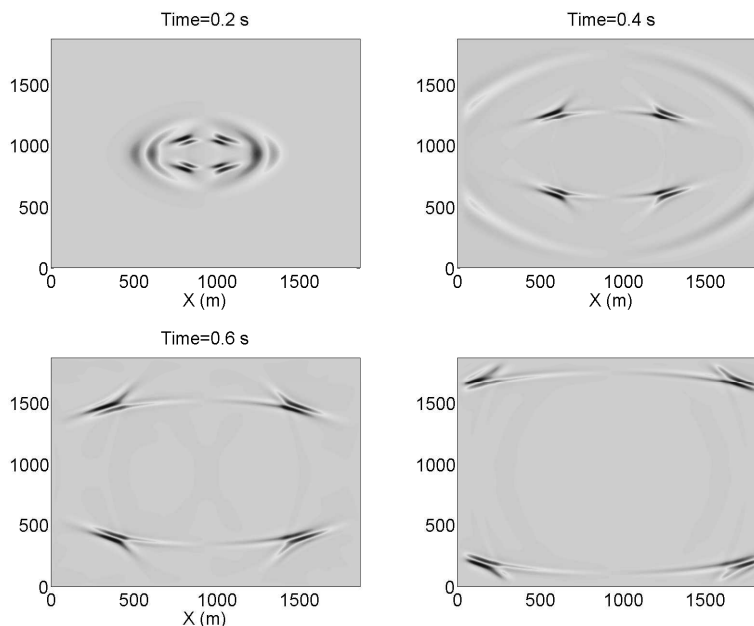
FIG. 4. Snapshots of stress component σ_{xx} for first-order velocity-stress wave equation set when H-PML is applied

In Figure (3), waveforms of normal stress components in the case of both C-PMLs (red dotted line) and H-PMLs (blue line) for absorbing the boundary wave are displayed. The results demonstrated the efficiency of the H-PML in comparison with the C-PML in this VTI model, especially when we zoom in the results from 0.6 s to 1.6 s, the stress components obtained by using C-PML suffer severely from the oscillations because of the boundary reflections.

In order to make a comparison with simulations of the first order velocity-stress wave equations, a point source with the Ricker wavelet of equation (19) is added on velocity component in X direction. The normal stress components can thus be obtained by the first order velocity-stress staggered-grid finite difference method with H-PML. Snapshots of the simulations are shown in Figure (5), which are almost the same with those in Figure (4) calculated by the first-order wave equations.

In Figure (6), waveforms of normal stress components in the case of both first order velocity-stress wave equations (blue line) and second order displacement-stress wave equations (red line) with H-PMLs are displayed. For different receivers, the normal stress components both in X direction (Left) and in Z direction (Right) match quite well for the two different wave equation sets. The results demonstrated the efficiency of the H-PML in both the wave equation sets.

Thrust fault model for second-order wave equations using H-PML

The next example is the simplified anisotropic thrust fault model, in which anisotropy presents through different depth intervals. In Figure (7), a vertical source is located in
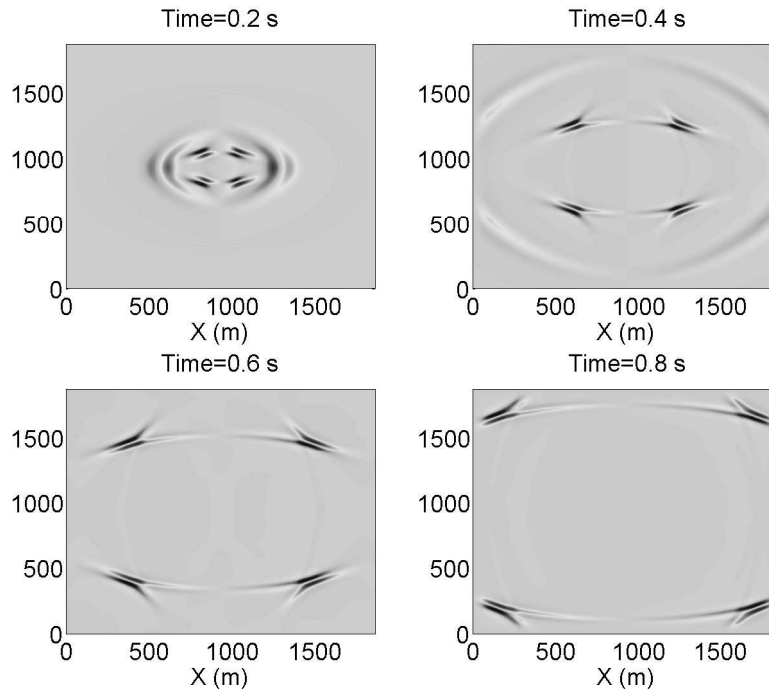
FIG. 5. Snapshots of stress component σ_{xx} for second-order displacement-stress wave equation set when H-PML is applied
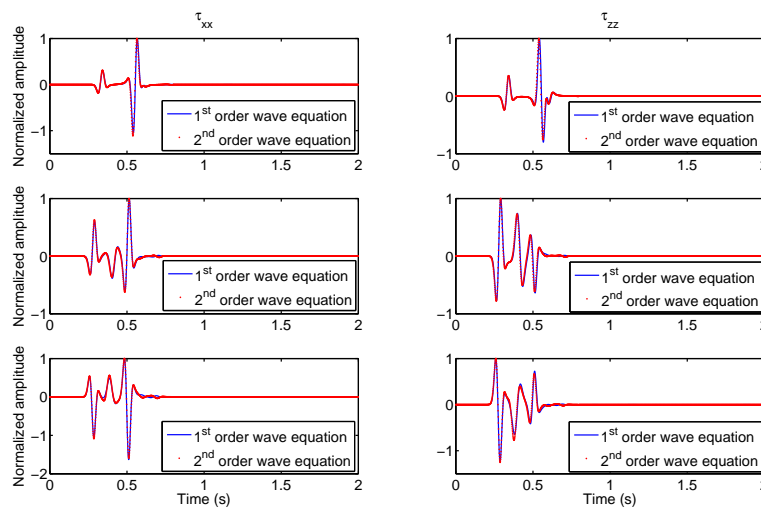

FIG. 6. Waveform comparison of second-order and first-order velocity-stress elastic wave equation sets when H-PML is applied in anisotropic media. H-pml works well in both first- and second-order elastic wave equations.

the upper middle of the fault. With the propagation time increasing, the waveform travels through the model to the boundaries, however, no boundary reflections can be found in each time slice. And the waveforms are absorbed when they travel into the PMLs.
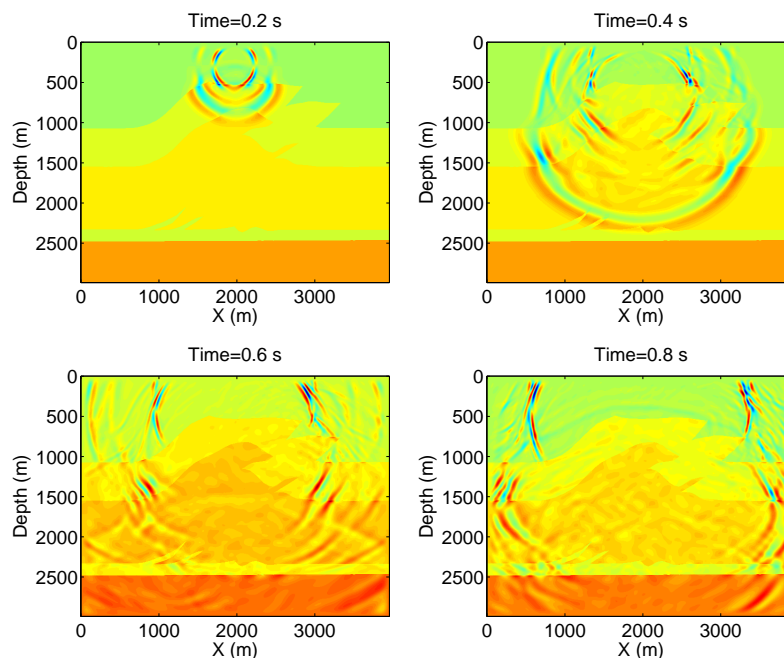

FIG. 7. Waveform snapshots with the increase of propagation time.

In figure (8), the seismograms of stress components σ_{xx} and σ_{zz} show the boundary reflections are effectively suppressed. The receiver stations are evenly spaced along x-direction with a same depth of the source.

CONCLUSIONS

In this paper, the H-PML is modified to be applied for suppression of the artificial boundary reflections in second-order wave equations. Its results in both isotropic and anisotropic medium are compared with those of the C-PML approach for the second-order wave equations. The simulation results of the H-PML for first-order and second-order wave equations are also compared. The H-PML can provide satisfying absorbing efficiency for both first and second-order elastic wave equations. And both of the two PMLs are stable and efficient in isotropic medium, yet, instability can be observed in anisotropic medium when C-PML is applied.
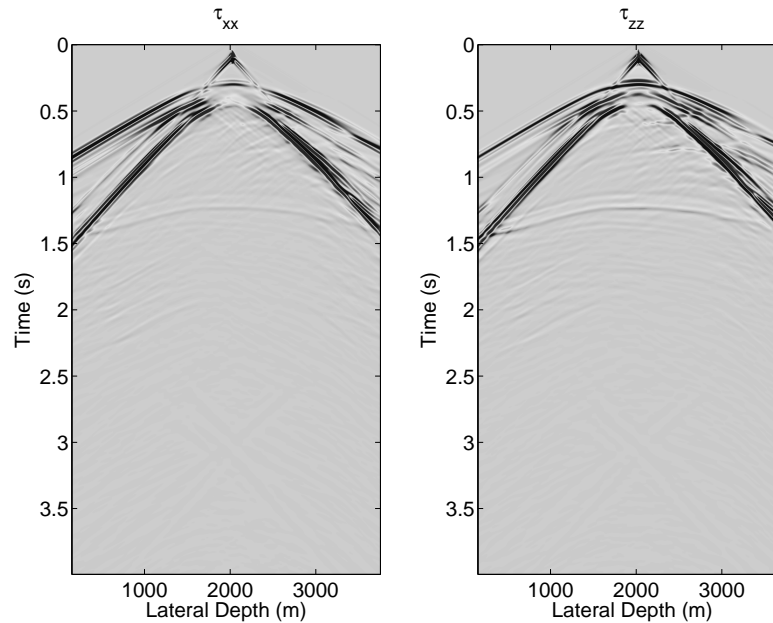
ACKNOWLEDGMENTS

FIG. 8. Seismograms of stress components σ_{xx} and σ_{zz}

REFERENCES

Berenger, J.-P., 1994, A perfectly matched layer for the absorption of electromagnetic waves: Journal of computational physics, **114**, No. 2, 185–200.

Bérenger, J.-P., 2002, Application of the cfs pml to the absorption of evanescent waves in waveguides: IEEE Microwave and Wireless Components Letters, **12**, No. 6, 218–220.

Collino, F., and Tsogka, C., 2001, Application of the perfectly matched absorbing layer model to the linear elastodynamic problem in anisotropic heterogeneous media: Geophysics, **66**, No. 1, 294–307.

Festa, G., and Vilotte, J.-P., 2005, The newmark scheme as velocity–stress time-staggering: an efficient pml implementation for spectral element simulations of elastodynamics: Geophysical Journal International, **161**, No. 3, 789–812.

Komatitsch, D., and Martin, R., 2007, An unsplit convolutional perfectly matched layer improved at grazing incidence for the seismic wave equation: Geophysics, **72**, No. 5, SM155–SM167.

Komatitsch, D., and Tromp, J., 2003, A perfectly matched layer absorbing boundary condition for the second-order seismic wave equation: Geophysical Journal International, **154**, No. 1, 146–153.

Kuzuoglu, M., and Mittra, R., 1996, Frequency dependence of the constitutive parameters of causal perfectly matched anisotropic absorbers: Microwave and Guided Wave Letters, IEEE, **6**, No. 12, 447–449.

Li, J., Innanen, K. A., Tao, G., Zhang, K., and Lines, L., 2017, Wavefield simulation of 3d borehole dipole radiation: Geophysics, **82**, No. 3, D155–D169.

Li, Y., and Bou Matar, O., 2010, Convolutional perfectly matched layer for elastic second-order wave equation: The Journal of the Acoustical Society of America, **127**, No. 3, 1318–1327.

Liu, Y.-s., Liu, S.-l., Zhang, M.-g., and Ma, D.-t., 2012, An improved perfectly matched layer absorbing boundary condition for second order elastic wave equation: Progress in Geophysics, **27**, 2113–2122.

Meza-Fajardo, K. C., and Papageorgiou, A. S., 2008, A nonconvolutional, split-field, perfectly matched layer for wave propagation in isotropic and anisotropic elastic media: stability analysis: Bulletin of the Seismological Society of America, **98**, No. 4, 1811–1836.

Ping, P., Zhang, Y., and Xu, Y., 2014, A multiaxial perfectly matched layer (m-pml) for the long-time simulation of elastic wave propagation in the second-order equations: Journal of Applied Geophysics, **101**, 124–135.

Pinton, G. F., Dahl, J., Rosenzweig, S., and Trahey, G. E., 2009, A heterogeneous nonlinear attenuating full-wave model of ultrasound: IEEE transactions on ultrasonics, ferroelectrics, and frequency control, **56**, No. 3.

Roden, J. A., and Gedney, S. D., 2000, Convolutional pml (cpml): An efficient fdtd implementation of the cfs-pml for arbitrary media: Microwave and optical technology letters, **27**, No. 5, 334–338.